Journal of
Polymer Materials

Tech Science Press

https://doi.org/10.32604/jpm.2026.073588

ARTICLE

Preparation of ZnO Nanoparticles Incorporated into Cross-Linked Poly (Methyl Methacrylate) (PMMA) Polymer and Its Biological Application

Nazeeha S. Alkayal*

Chemistry Department, Faculty of Science, King Abdulaziz University, Jeddah, Saudi Arabia

*Corresponding Author: Nazeeha S. Alkayal. Email: nalkayal@kau.edu.sa

Received: 21 September 2025; Accepted: 23 January 2026; Published: 03 April 2026

ABSTRACT: The development of polymer nanoparticle composites with enhanced thermal and antibacterial properties is essential for next-generation biomedical materials. However, conventional polymers often exhibit limited bioactivity and poor resistance to degradation, restricting their functional applications. The novelty of this study involves the combination of the bio-derived cross-linker 2,5-bis(aminomethyl)furan (BAF) into poly (methyl methacrylate) PMMA to form a cross-linked network incorporated with various ratios of ZnO nanoparticles (ZnO NPs), resulting in improved biological and thermal properties. The surface morphologies, material crystallinity, and thermal degradation properties of the synthesized BAF–PMMA/ZnO were investigated using Scanning Electron microscopy (SEM), Energy-Dispersive X-ray spectroscopy (EDX), X-ray diffraction (XRD), and Thermogravimetric characterization technique (TGA), respectively. The prepared BAF-PMMA/ZnO nanocomposites showed an enhancement in the crystallinity after increasing the ratio of ZnO NPs compared to the amorphous cross-linked BAF–PMMA polymer. The thermal stability of nanocomposites was significantly enhanced after the introduction of ZnO NPs into cross-linked BAF–PMMA polymer. The resultant nanocomposites BAF–PMMA/ZnO were examined as antibacterial agents against the *Escherichia coli* (*E. coli*) and *Staphylococcus aureus (S. aureus)* bacterial strains. The results showed that most BAF–PMMA/ZnO nanocomposites have antibacterial activity against both bacterial species compared to the pure cross-linked BAF-PMMA polymer. The BAF–PMMA/ZnO 10 wt.% sample shows the highest inhibition zone of (16.3 ± 0.33) against *E. coli*. These outcomes demonstrate that such nanocomposites offer a viable pathway toward multipurpose biomaterials with exceptional structural and biological features.

KEYWORDS: Cross-linked PMMA; furan; ZnO nanoparticle; antibacterial; *E. coli*; *S. aureus*

1 Introduction

Poly (methyl methacrylate) (PMMA) is a multifunctional thermoplastic that is prized for its biocompatibility, chemical resistance, optical clarity, and thermal stability [1]. It is extensively utilized in drug delivery, dentistry, orthopedics, biomedical devices, and optoelectronics. Nevertheless, PMMA has limited mechanical strength and brittleness, especially at high temperatures. These restrictions are improved by crosslinking with multifunctional agents, opening new possibilities for wastewater treatment, electronics, sensors, and pharmaceuticals [1,2].

Nanocomposites have become an important class of innovative materials because they combine the functional benefits of inorganic nanoparticles with the unique features of polymers [1]. These hybrid materials, which are created by introducing nanoscale fillers into polymeric matrices, frequently have improved rigidity, thermal resistance, optical properties, and biological activity when compared to their

pure counterparts [3,4]. The high surface-to-volume ratio and distinct physicochemical characteristics of nanoparticles, which permit robust interfacial interactions with the host polymer, are the causes of these enhancements [5]. Nanocomposites have found widespread uses in environmental remediation, biomedical engineering, catalysis, and antimicrobial coatings as a result of these synergies [6,7].

Metal oxide nanoparticles were used as fillers for the enhancement of polymer-based nanocomposites [8,9]. Zinc Oxide nanoparticles (ZnO NPs), as one of the versatile inorganic nanomaterials, have drawn more attention recently because of their numerous significant physical and chemical characteristics, such as chemical stability [10,11], remarkable optical transparency [12], high photocatalytic activity [13], and potent antibacterial and bactericide properties [14,15]. Due to their small size, high specific area, quantum influence, and strong interactions between the organic polymer and inorganic nanoparticles, ZnO NPs have the potential to enhance the thermal and optical performance of PMMA polymer matrices [16,17]. Therefore, these nanocomposites could be employed in dental prosthetics, bone cement, contact lenses, and antimicrobial coatings [18,19]. There are numerous examples that clarify the effectiveness of modifying polymeric materials with ZnO NPs. One study, for example, focused on creating a novel polymer with ZnO NPs [20]. It was discovered that the ZnO nanoparticles and the different polymer matrices had excellent interfacial contact, which improved the material's mechanical qualities [21]. Additionally, another work produced a PMMA/ZnO hybrid system and validated its advantageous application for photocatalytic activity [7]. Furthermore, researchers examined the antibacterial properties of polyacrylate/ZnO nanocomposites comprising various ZnO nanoparticle morphologies and discovered that those having sphere-like and flower-like ZnO NPs had superior antibacterial properties [22].

In this work, 2,5-bis(aminomethyl)furan (BAF) was proposed as a bifunctional cross-linking agent to modify the properties of PMMA and incorporated with different concentrations of ZnO NPs ranging from 2% to 20% into the polymer matrix. ZnO nanoparticles were selected over other metal oxide nanoparticles, such as Ag, TiO_2, or Cu, due to their antimicrobial activity, environmental safety, low toxicity, and cost. This modification improves rigidity, thermal stability, and biological performance. As a result, the selection of BAF–PMMA/ZnO nanocomposites in this study was based on making it a promising material for potential biomedical and environmental applications.

2 Materials and Methods

2.1 Materials

PMMA was procured from Across Organics, Geel, Belgium. BAF, 98% was supplied by Baoji Guokang Biotechnology, Ltd., Baoji, China, while tetrahydrofuran (THF, 99.9%) was obtained from Merck KGaA, Darmstadt, Germany. ZnO nanoparticles were commercially obtained (Sigma-Aldrich, St. Louis, MO, USA <100 nm, purity > 99%). All compounds were utilized without additional purification.

2.2 Instrumental

Thermo-gravimetric analysis (TGA) was performed on a TGA4724 with a heating rate of 10°C/min between 25°C and 500°C under N_2 atmosphere. Fourier transform infrared spectra (FTIR) with a Nicolet Magna 6700 FT spectrometer were conducted in a wavenumber region (400–4000 cm^{-1}). X-ray diffraction (XRD) patterns were studied using a Bruker D8 Advance with Cu Kα radiation (wavelength 1.5418 Å) at 40 kV and 40 mA. The patterns were collected between 2θ of 10° and 60°, and the scan speed was 1.5°/min. Scanning electron microscopy (SEM) imaging was performed with a FEI TENEO VS microscope equipped with an EDAX detector.

2.3 Preparation of BAF–PMMA/ZnO Nanocomposites

BAF–PMMA/ZnO nanocomposite materials were prepared by an *in-situ* polymerization technique as follows: 1 g of PMMA was dissolved in THF solvent (50 mL). 2,5-Bis(aminomethyl)furan (BAF) was used as a cross-linking agent. A fixed amount of 0.20 g of BAF (1.59 mmol), corresponding to 13.7 mol% relative to PMMA repeat units (1.00 g, 9.99 mmol), was added to the reaction mixture prior to *in-situ* polymerization. Then ZnO nanoparticles with different ratios (2, 5, 10, 20 wt.%) were dispersed through the PMMA solution by stirring, before being ultrasonicated for 10 min. Finally, the cross-linker BAF was added, and the mixture was refluxed for about 8 h at 70°C with regular shaking. The resulting mixture was then poured into petri dishes and left to dry for 24 h at 25°C. The samples were designated as presented in Table 1.

Table 1: Chemical compositions of bare BAF–PMMA and BAF–PMMA/ZnO nanocomposites.

Entry	Sample	BAF (g)	PMMA (g)	ZnO (g)
1	BAF–PMMA	0.2 g	1 g	0
2	BAF–PMMA/ZnO 2%			0.02
3	BAF–PMMA/ZnO 5%			0.05
4	BAF–PMMA/ZnO 10%			0.1
5	BAF–PMMA/ZnO 20%			0.2

2.4 The Antibacterial Activities of BAF–PMMA/ZnO Nanocomposites

A Disk diffusion susceptibility test was utilized to examine the antibacterial effects of BAF-PMMA and BAF-PMMA/ZnO nanoparticles compared to Tetrahydrofuran (THF), ZnO as negative controls, and Gentamicin (Mast diagnostics, Ltd., Bootle, UK) as a positive control using Müeller-Hinton agar (Difco, Laboratories, Detroit, MI, USA) plates. Gentamicin was selected as it inhibits a wide spectrum, affecting both Gram-negative and Gram-positive bacteria. Gram-negative bacteria, *Escherichia coli* (ATCC 11775), and Gram-positive bacteria, *Staphylococcus aureus* (ATCC 12600), were selected. The bacterial strains were subcultured by inoculating them in Nutrient Broth (Oxoid Ltd., Basingstoke, UK) for 18 h to ensure the bacteria were in the log phase. Then, around 8 mm of nanoparticles were prepared in Disks, followed by adding them to Müeller-Hinton agar after streaking with bacteria. Plates were incubated at 37°C for 24 h before measuring the inhibition zones in millimeters (mm) using a caliper (Memmert GmbH + Co. KG, Schwabach, Germany). The charts were created using GrapPad Prism (version 10.6.0), which included triple readings. Two-way ANOVA was performed, followed by Dunnett's multiple comparisons test to compare between groups. Using Gentamicin as a positive control to compare with all other bacterial treatments. The dried films were cut into circular discs (8 mm in diameter); each treatment was tested on at least three independent plates (n = 3), and the areas of inhibition were measured in millimeters using a calibrated digital scale (Mitutoyo Corporation, Kawasaki, Japan).

3 Results and Discussions

3.1 Morphological and Elemental Investigation

BAF–PMMA/ZnO nanocomposite materials were prepared by an *in-situ* polymerization technique as illustrated in scheme 1. The surface morphologies of pure BAF–PMMA cross-linked polymer exhibited a microporous structure as illustrated in Fig. 1a,b. Therefore, the SEM images of the prepared nanocomposites BAF–PMMA/ZnO revealed porous morphology on the polymer matrix, which can increase the surface area and help with the good distribution of ZnO NPs. The porosity measurement was not quantitative in

this work and is planned for future study to correlate the effect of porosity with the application. The SEM micrographs (Fig. 1c–j) illustrate the effect of varying ZnO NPs ratios (2–20 wt.%). In the BAF–PMMA/ZnO nanocomposites, the bright regions correspond to ZnO NPs, indicating their presence both on the surface and within the pores of the polymeric network, as shown in Fig. 1c–j. When the concentration of ZnO NPs increases from 2 to 20 wt.%, noticeable agglomeration is observed. This aggregation is attributed to the high surface energy and strong interparticle attractions of the nanoparticles, which promote clustering at higher concentrations [23].

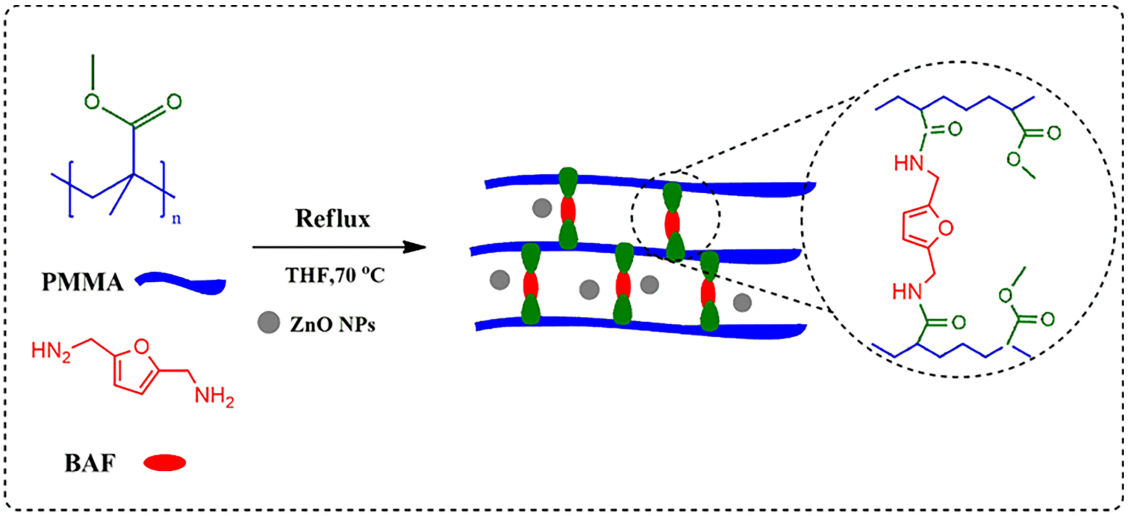

Scheme 1: Schematic diagram for the BAF–PMM/ZnO nanocomposites polymer fabrication.

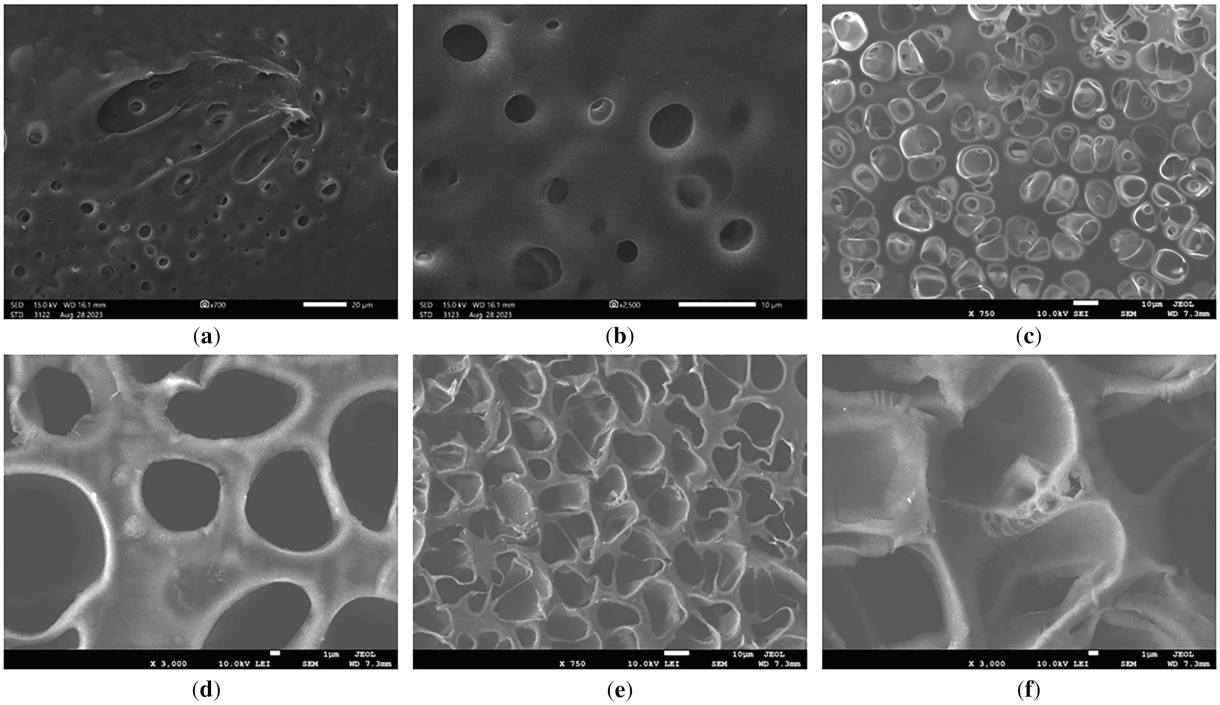

(**a**) (**b**) (**c**)

(**d**) (**e**) (**f**)

Figure 1: (Continued)

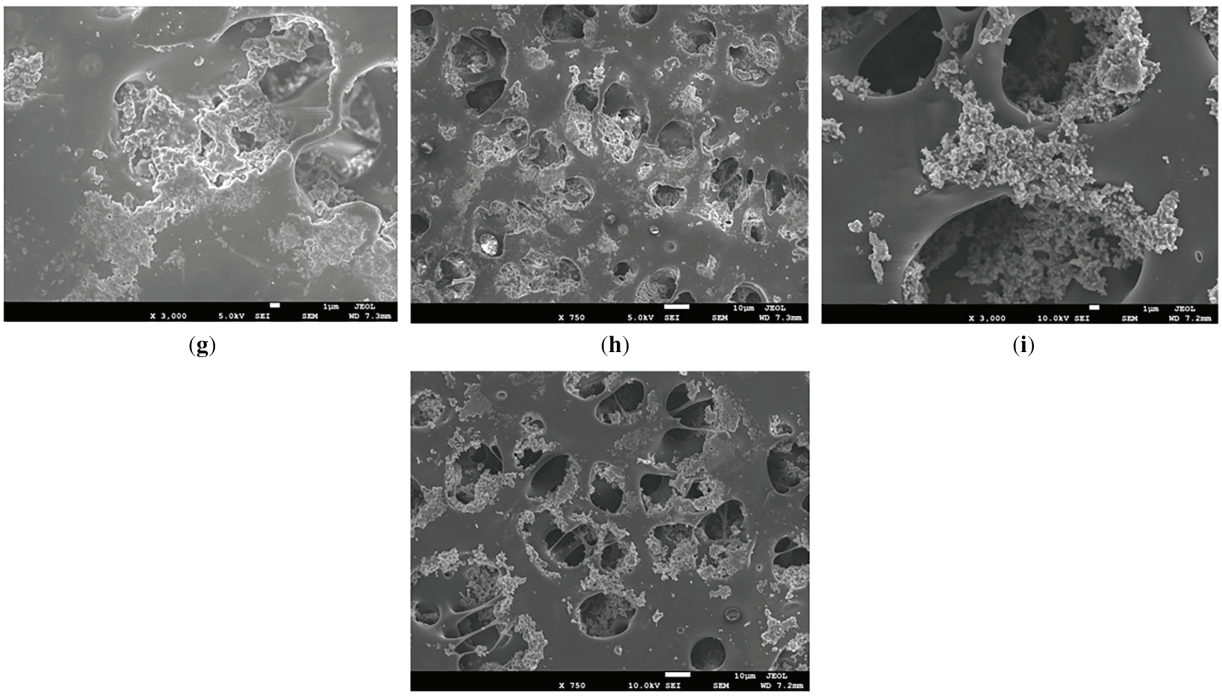

(**g**) (**h**) (**i**)

(**j**)

Figure 1: SEM images at two magnifications for (**a**,**b**) BAF–PMMA, (**c**,**d**) BAF–PMMA/ZnO 2%, (**e**,**f**) BAF–PMMA/ZnO 5%, (**g**,**h**) BAF–PMMA/ZnO 10%, and (**i**,**j**) BAF–PMMA/ZnO 20%.

The elemental composition of the prepared BAF–PMMA/ZnO nanocomposites was investigated using Energy Dispersive X-ray (EDX) analysis. The EDX of the bare BAF-PMMA was illustrated in Fig. S1, which demonstrates the characteristic signals corresponding to carbon (C), nitrogen (N), and oxygen (O). As shown in Fig. 2a,b for samples containing 2 and 5 wt.% ZnO, respectively, the EDX spectra exhibited only two characteristic signals corresponding to carbon (C) and oxygen (O), with no detectable Zn peaks. This absence may be attributed to the low concentration of ZnO nanoparticles and their inhomogeneous dispersion within the cross-linked polymer matrix, as well as the surface-sensitive and localized nature of EDX analysis [24,25]. In contrast, at higher ratios from ZnO 10 and 20 wt.% (Fig. 2c,d), distinct Zn signals appeared alongside the C and O peaks, confirming the presence of ZnO nanoparticles in the nanocomposites. These findings reveal the outstanding purity of the synthesized materials and show that their elemental composition is in line with the intended formula. Table 2 summarizes the elemental contents of the BAF–PMMA/ZnO (1–4) nanocomposites.

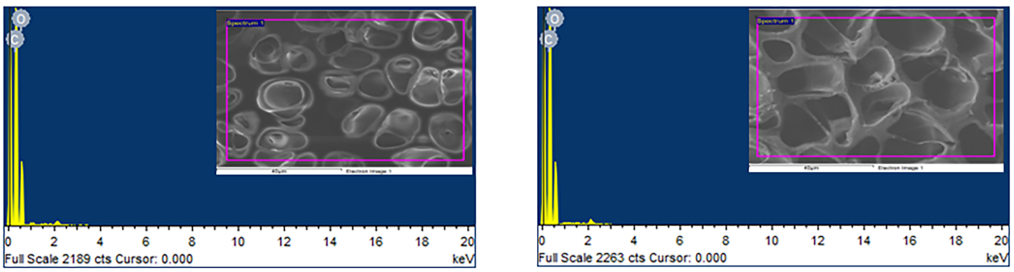

(a) **(b)**

Figure 2: (Continued)

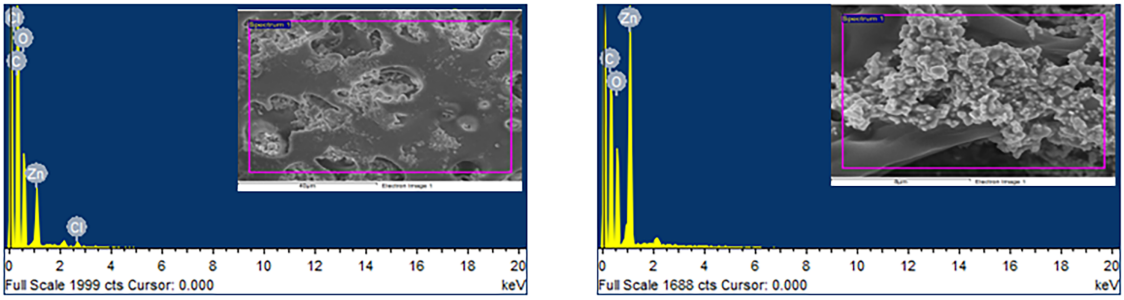

Figure 2: EDX analysis of (**a**) BAF–PMMA/ZnO 2%, (**b**) BAF–PMMA/ZnO 5%, (**c**) BAF–PMMA/ZnO 10%, and (**d**) BAF–PMMA/ZnO 20%.

Table 2: Elemental composition of the BAF–PMMA/ZnO (1–4) nanocomposites.

Sample	Element	Weight %	Atomic %
BAF–PMMA/ZnO 2%	C K	64.53	70.79
	O K	35.47	29.21
BAF–PMMA/ZnO 5%	C K	64.77	71.01
	O K	35.23	28.99
BAF–PMMA/ZnO 10%	C K	58.82	71.59
	O K	27.50	25.12
	Zn L	12.45	2.78
BAF–PMMA/ZnO 20%	C K	42.84	66.30
	O K	19.88	32.09
	Zn L	37.29	10.60

3.2 Structural Investigation

X-ray diffraction analysis was performed to examine the crystal structure of the prepared BAF–PMMA/ZnO nanocomposites over a 2θ range of 5°–60°. The diffraction patterns for BAF-PMMA and all prepared BAF-PMMA/ZnO nanocomposites are presented in Fig. 3. The bare BAF–PMMA exhibits an amorphous nature, as indicated by the broad peaks centered around 2θ values of 15°, 30°, and 43°. Upon the incorporation of ZnO nanofillers, notable changes in the crystallinity of the cross-linked BAF–PMMA polymer were observed. Specifically, sharp and intense diffraction peaks appeared at 2θ values of 31.7°, 34.4°, 36.1°, 47.5°, 56.5°, 62.8°, 66.3°, 67.9°, and 69°, which are consistent with the standard pattern of hexagonal wurtzite ZnO (JCPDS Card No. 36-1451) [26]. The intensity of these peaks progressively increased with rising ZnO ratios (2–20 wt.%) in the polymer matrix. These observations not only confirm the successful incorporation of ZnO nanoparticles into the cross-linked BAF–PMMA polymer but also demonstrate that ZnO contributes to enhancing the overall crystallinity of the nanocomposite matrix. The crystallinity % are 5.44, 3.14, 1.83, and 1.07 for BAF-PMMA/Zno 20%, BAF-PMMA/ZnO 10%, BAF-PMMA/ZnO 5% and BAF-PMMA/ZnO 2%, respectively. In this study, the XRD discussion demonstrated that the crystallinity of ZnO NPs in the polymer matrix increases with the rise in the ratios of ZnO NPs. The crystalline size and lattice strain behavior of ZnO NPs within the BAF–PMMA matrix will be calculated using the Scherrer equation or Williamson-Hall analysis for further investigation in future work.

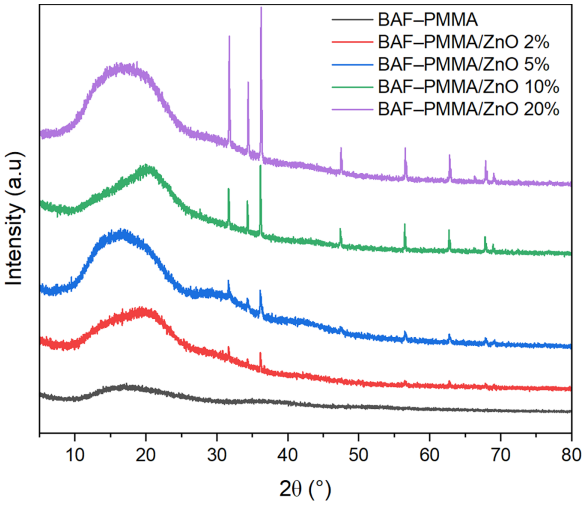

Figure 3: The XRD patterns of bare BAF–PMMA and BAF–PMMA/ZnO nanocomposites.

The Fourier-Transform Infrared spectra of the prepared BAF–PMMA/ZnO nanocomposites were recorded in the range of 4000–500 cm^{-1}, as presented in Fig. 4. The spectra revealed characteristic absorption bands corresponding to the polymer precursors, namely PMMA and the cross-linker aminomethyl furan [27]. The successful formation of the cross-linked polymer was confirmed by the sharp absorption band at 1721 cm^{-1}, attributed to the C=O stretching vibration of the acrylate ester group in PMMA. Furthermore, the transformation of primary amino groups ($R–NH_2$) in aminomethyl furan into secondary amino groups (N–H) was verified by the appearance of a singlet stretching vibration band at 3383 cm^{-1} in the final cross-linked polymer. FT-IR analysis confirmed that the polymer retained its original bonding framework, showing no evidence of bond cleavage or the formation of new functional groups after ZnO NPs incorporation.

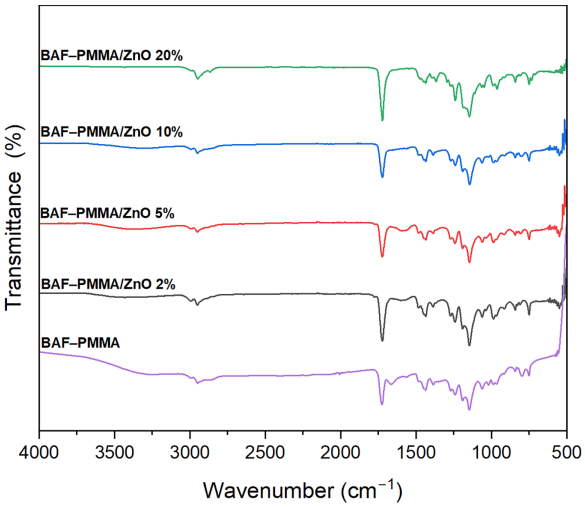

Figure 4: FT-IR spectra of bare BAF–PMMA and BAF–PMMA/ZnO nanocomposites.

3.3 Thermogravimetric Analysis

The thermal stability of the prepared BAF–PMMA/ZnO nanocomposites was investigated to evaluate the influence of ZnO nanoparticle incorporation and concentration on the stability of the BAF–PMMA

polymer. As shown in Fig. 5, the TGA curves of all nanocomposites revealed three distinct degradation stages, observed at both low and high ZnO. At lower ZnO contents (2 and 5 wt.%), the first stage corresponds to a 5% weight loss of around 152°C, followed by a 10% weight loss near 184°C in the second stage, and a major 50% weight loss at approximately 353°C in the third stage. At higher ZnO (10 and 20 wt.%), degradation also occurred in three stages, with 5% weight loss in the temperature range of 153°C–165°C, 10% weight loss in the 235°C–246°C range, and a significant 60% weight loss at around 406°C. The initial degradation step is attributed to the evaporation of absorbed water molecules. The second degradation stage is attributed to the breakdown of both cross-linking bonds and the polymer backbone. The third stage involves extensive decomposition and combustion, resulting in a 50%–60% weight loss. The maximum polymer decomposition temperature (T_{max}), which indicates the temperature at which the highest rate of weight loss occurs, was determined for all samples. In addition, the characteristic degradation temperatures T_{10}, T_{30}, and T_{50}—representing the temperatures at which 10%, 30%, and 50% mass loss occur, respectively—were also evaluated for the BAF–PMMA/ZnO nanocomposites as illustrated in Table 3.

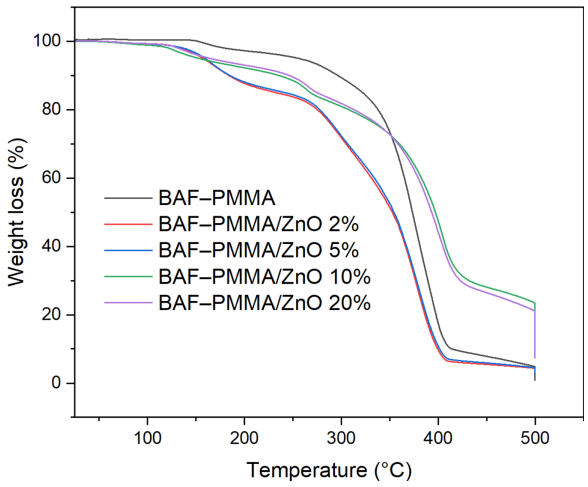

Figure 5: The TGA analysis of BAF–PMMA and BAF–PMMA/ZnO nanocomposites.

Table 3: Thermal properties of BAF–PMMA and BAF–PMMA/ZnO nanocomposites.

Sample	T_{10} (°C)	T_{30} (°C)	T_{50} (°C)	T_{max} (°C)
BAF–PMMA	281	354	373	401
BAF–PMMA/ZnO 2%	184	305	352	410
BAF–PMMA/ZnO 5%	185	305	354	410
BAF–PMMA/ZnO 10%	235	360	396	500
BAF–PMMA/ZnO 20%	246	360	392	500

The T_{max}, T_{10}, T_{30}, and T_{50} values of BAF–PMMA/ZnO nanocomposites with higher ZnO were consistently greater than those observed at lower contents, reflecting the higher decomposition resistance of the inorganic phase [27]. Moreover, the T_{max} values of the high ratio of ZnO NPs (500°C) were significantly higher than those reported for the cross-linked polymer without ZnO NPs in our previous work (393°C–412°C) [28]. Overall, these findings demonstrate a marked enhancement in the thermal stability of BAF–PMMA/ZnO nanocomposites compared with pure cross-linked polymer.

3.4 Antibacterial Activity of Polymers

The antibacterial performance of the prepared nanocomposites was evaluated against two representative bacterial strains: *Escherichia coli* ATCC 11775 (Gram-negative) and *Staphylococcus aureus* ATCC 12600 (Gram-positive) [28–30]. The antibacterial effects of BAF-PMMA in the presence or absence of increasing concentrations of ZnO (BAF-PMMA/ZnO) were assessed against gram-negative *E. coli* and gram-positive *S. aureus* bacteria. As shown in Fig. 6, BAF-PMMA alone exhibited no inhibitory effect on either bacterial strain, evidenced by the absence of inhibition zones around the polymer disks; therefore, a fixed concentration of 20% BAF-PMMA was selected for subsequent experiments.

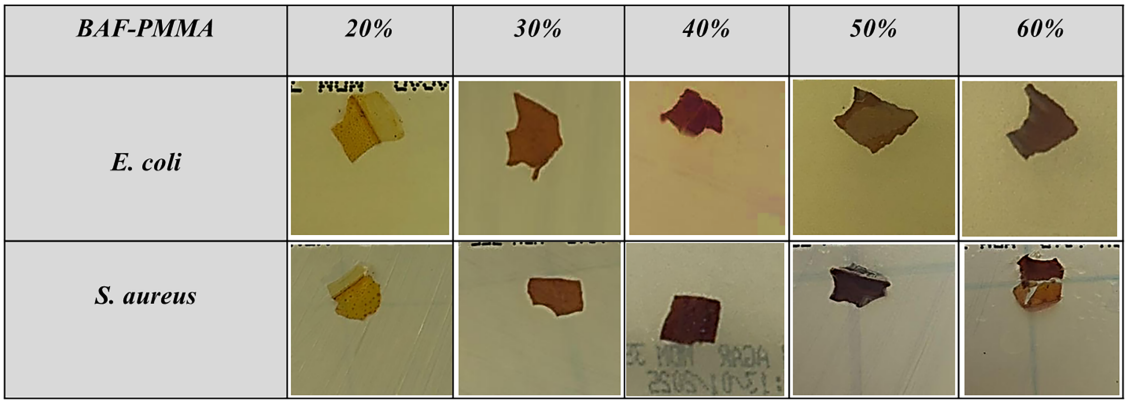

Figure 6: The effect of BAF-PMMA on *E. coli* and *S. aureus*. Different concentrations of BAF-PMMA (20%, 30%, 40%, 50%, and 60%) were examined using a Disk diffusion test for 24 h at 37°C.

Interestingly, increasing concentrations of ZnO (BAF-PMMA/ZnO) from 2% to 20% have inhibited bacterial growth. Results in Fig. 7 showed that the BAF-PMMA/ZnO nanoparticles have created an increasing diameter inhibiting zone of *E. coli* from (11.2 ± 0.6 mm) in 2% ZnO to (16.3 ± 0.33 mm) in 10% ZnO, with a sudden decrease in the inhibiting zone diameter of (9.6 ± 0.33 mm) in 20% ZnO. Interestingly, comparing BAF-PMMA/ZnO treated *E. coli* with Gentamicin as a positive control (17.4 ± 0.33 mm) shows no significance between the 2 groups, indicating that BAF-PMMA/ZnO 10% as strong as Gentamicin in inhibiting *E. coli*, with a p value = 0.723. Unlike all the other *E. coli*-treated cultures with THF, ZnO, BAF-PMMA, BAF-PMMA/ZnO 2%, BAF-PMMA/ZnO 5%, and BAF-PMMA/ZnO 20% separately, which show a p value of <0.0001, <0.0001, 0.0001, 0.001, 0.002, 0.0001, respectively.

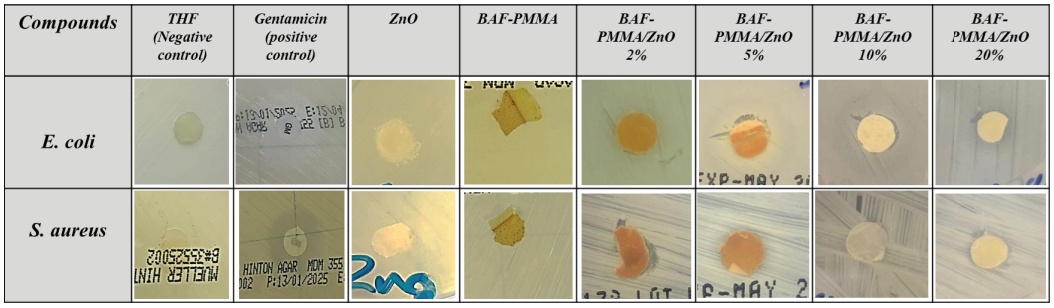

(**A**)

Figure 7: (Continued)

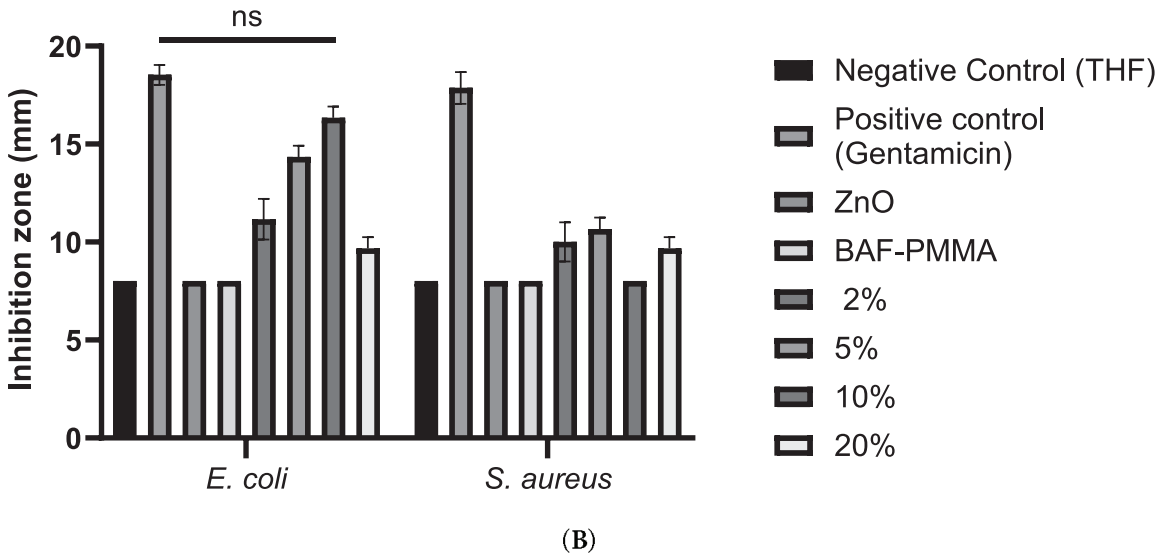

Figure 7: Antibacterial activity of BAF-PMMA/ZnO nanocomposites prepared using 20% BAF-PMMA cross-linked with varying ZnO concentrations (2%, 5%, 10%, and 20%) against *E. coli* and *S. aureus*. Treatments were compared with a negative control (THF), a positive control (Gentamicin), ZnO alone, and BAF-PMMA alone. Disk diffusion assays were performed on Müeller–Hinton agar plates inoculated with each bacterial strain, followed by incubation for 24 h at 37°C. (**A**) Representative inhibition zones produced by BAF-PMMA/ZnO against both bacterial species. (**B**) Bar graphs showing the mean inhibition zone diameters (mm), generated using GraphPad Prism. The data represents the average of three independent measurements. Statistical analysis was conducted using two-way ANOVA followed by Dunnett's multiple comparisons test, with Gentamicin used as the reference treatment. Significant differences were observed for all treatments compared with Gentamicin ($p < 0.002–0.0001$), except for *E. coli* treated with 10% BAF-PMMA/ZnO, which showed no significant (ns) difference relative to Gentamicin ($p = 0.723$).

The inhibition zones of *S. aureus* affected by BAF-PMMA/ZnO nanoparticles were less compared to *E. coli*. The highest inhibition zone of *S. aureus* was detected at (10.66 ± 0.33 mm) at 5% ZnO, and no effect at 10% ZnO. The distinct effects that BAF-PMMA/ZnO demonstrated against the two species of bacteria are due to structural variations between them. At higher loading of ZnO, the irregular response is most likely attributed to the aggregation/blocking of zinc oxide molecules, which reduces the proportion of surface-exposed molecules and limits the diffusion of active species in the agar diffusion assay. This interpretation will be confirmed by dispersion mapping and zinc (Zn^{2+}) ion release measurements in future studies.

The equilibrium and integrity of the bacterial cell wall, which displays anti-microbial activity towards microorganisms, may be disrupted by the BAF-PMMA/ZnO resin due to the electrostatic interaction between the positively charged resin and the negatively charged bacterial cell membrane. Furthermore, the free radicals on the resin surface may disrupt the lipids and structure of the microorganism cells' membranes, impairing their ability to function. Because of ZnO is incorporated within a PMMA cross-linked polymer network, the antibacterial effect is expected to be controlled by surface-exposed ZnO and limited Zn^{+2} diffusion; direct ROS/Zn^{+2} release assays were not achieved in this study and are planned for future work.

A comparative study of various commercial metal oxide nanoparticles was presented in Table 4. Common metal oxide nanoparticles have strong photocatalytic and antimicrobial properties. However, they often have challenges such as cytotoxicity, agglomeration, or the need for UV activation. In contrast, the prepared BAF-PMMA/ZnO nanocomposite approach a balanced combination of thermal stability, bio-derived cross-linker, biocompatibility, enhanced ZnO dispersion, and antimicrobial activity. The present

findings display that the BAF–PMMA/ZnO nanocomposite is a promising material for potential biomedical and environmental applications.

Table 4: Comparison of metal oxide nanoparticles and BAF–PMMA/ZnO nanocomposite based on previous studies.

Nanomaterial	Main Strengths	Main Limitations	References
ZnO	Strong antibacterial activity, UV protection, low cost, Biocompatible.	Cytotoxic at high doses, light-dependent activity	[31]
TiO_2	Chemically stable, photocatalytic, safe for biomedical use.	Requires UV activation, limited dark activity	[32]
Ag	Highly potent antimicrobial, effective at low doses.	Costly, possible cytotoxicity, and resistance issues	[33]
CuO	Cost-effective, good antibacterial activity in the dark.	Higher cytotoxicity, stability issues	[34]
ZnO/TiO_2	Synergistic antimicrobial and photocatalytic effects.	Complex synthesis, potential polymer degradation	[35]
CuO/TiO_2	Visible-light antibacterial action, stable.	Increase cytotoxicity	[36]
ZnO/CuO	Strong antibacterial effect.	Requires precise composition control	[37]
BAF–PMMA/ZnO	Bio-derived cross-linker (BAF) improved thermal stability, enhanced dispersion and reduced agglomeration of ZnO nanoparticles, antibacterial improvement, particularly against *E. coli* and *S. aureus*, attributed to controlled Zn^{2+} exposure and porous morphology (inhibition zone 16.3 ± 0.33 mm vs *E. coli*).	Needs further cytotoxicity and long-term studies	This work

4 Conclusion

In this study, cross-linked BAF–PMMA/ZnO nanocomposites were successfully synthesized via an *in-situ* polymerization approach and evaluated for antibacterial activity against *Staphylococcus aureus* (Gram-positive) and *Escherichia coli* (Gram-negative). Comprehensive structural, thermal, and morphological characterizations demonstrated that ZnO nanoparticles were effectively incorporated within the polymer matrix, as clearly shown by the XRD diffraction peaks and EDX compositional mapping. The addition of ZnO nanoparticles significantly improved the thermal stability of the BAF–PMMA polymer. Moreover, the nanocomposites exhibited superior antibacterial performance compared to pristine BAF–PMMA, with particularly strong inhibition against *E. coli*, showing inhibition zones ranging from 9.6 ± 0.33 to 16.3 ± 0.33 mm.

Acknowledgement: The author acknowledges Dr. Fatemah Salem Basingab from the biology department at King Abdulaziz University for her support in biological study.

Funding Statement: Not applicable.

Availability of Data and Materials: This article does not involve data availability, and this section is not applicable.

Ethics Approval: Not applicable.

Conflicts of Interest: The author declares no conflicts of interest.

Supplementary Materials: The supplementary material is available online at https://www.techscience.com/doi/10.32604/jpm.2026.073588/s1.

References

1. Alkayal NS. Fabrication of cross-linked PMMA/SnO_2 nanocomposites for highly efficient removal of chromium (III) from wastewater. Polymers. 2022;14(10):2101. doi:10.3390/polym14102101.
2. Poddar MK, Sharma S, Moholkar VS. Sonochemical synthesis of PMMA/cloisite 30B nanocomposites: a mechanistic investigation. Macromol Symp. 2016;361(1):82–100. doi:10.1002/masy.201500009.
3. Liu P, Su Z. Preparation and characterization of PMMA/ZnO nanocomposites via *in-situ* polymerization method. J Macromol Sci Part B Phys. 2006;45(1):131–8. doi:10.1080/00222340500408085.
4. Poddar MK, Sharma S, Moholkar VS. Investigations in two-step ultrasonic synthesis of PMMA/ZnO nanocomposites by *in-situ* emulsion polymerization. Polymer. 2016;99(1):453–69. doi:10.1016/j.polymer.2016.07.052.
5. Khlifi K, Atallah MS, Cherif I, Karkouch I, Barhoumi N, Attia-Essaies S. Synthesis of ZnO nanoparticles and study of their influence on the mechanical properties and antibacterial activity of PMMA/ZnO composite for orthotic devices. Surf Interfaces. 2023;41(2):103279. doi:10.1016/j.surfin.2023.103279.
6. Di Mauro A, Cantarella M, Nicotra G, Pellegrino G, Gulino A, Brundo MV, et al. Novel synthesis of ZnO/PMMA nanocomposites for photocatalytic applications. Sci Rep. 2017;7(1):40895. doi:10.1038/srep40895.
7. Di Mauro A, Farrugia C, Abela S, Refalo P, Grech M, Falqui L, et al. Synthesis of ZnO/PMMA nanocomposite by low-temperature atomic layer deposition for possible photocatalysis applications. Mater Sci Semicond Process. 2020;118:105214. doi:10.1016/j.mssp.2020.105214.
8. Canché-Escamilla G, Duarte-Aranda S, Toledano M. Synthesis and characterization of hybrid silica/PMMA nanoparticles and their use as filler in dental composites. Mater Sci Eng C. 2014;42:161–7. doi:10.1016/j.msec.2014.05.016.
9. Wahab R, Hwang IH, Kim YS, Musarrat J, Siddiqui MA, Seo HK, et al. Non-hydrolytic synthesis and photo-catalytic studies of ZnO nanoparticles. Chem Eng J. 2011;175:450–7. doi:10.1016/j.cej.2011.09.055.
10. Sadeghi B. Preparation of ZnO/Ag nanocomposite and coating on polymers for anti-infection biomaterial application. Spectrochim Acta Part A Mol Biomol Spectrosc. 2014;118:787–92. doi:10.1016/j.saa.2013.09.022.
11. Khairy M, Amin NH, Kamal R. Optical and kinetics of thermal decomposition of PMMA/ZnO nanocomposites. J Therm Anal Calorim. 2017;128(3):1811–24. doi:10.1007/s10973-016-6062-x.
12. Dadi R, Azouani R, Traore M, Mielcarek C, Kanaev A. Antibacterial activity of ZnO and CuO nanoparticles against gram positive and gram-negative strains. Mater Sci Eng C. 2019;104:109968. doi:10.1016/j.msec.2019.109968.
13. Mendes CR, Dilarri G, Forsan CF, de Moraes Ruy Sapata V, Lopes PRM, de Moraes PB, et al. Antibacterial action and target mechanisms of zinc oxide nanoparticles against bacterial pathogens. Sci Rep. 2022;12:2658. doi:10.1038/s41598-022-06657-y.
14. Sirelkhatim A, Mahmud S, Seeni A, Kaus NHM, Ann LC, Bakhori SKM, et al. Review on zinc oxide nanoparticles: antibacterial activity and toxicity mechanism. Nano Micro Lett. 2015;7(3):219–42. doi:10.1007/s40820-015-0040-x.
15. Behera SK, Khan GA, Singh SS, Jena B, Sashank K, Patnaik S, et al. Antibacterial efficacy of ZnO/bentonite (clay) nanocomposites against multidrug-resistant *Escherichia coli*. ACS Omega. 2024;9(2):2783–94. doi:10.1021/acsomega.4c00630.
16. Motelica L, Vasile BS, Ficai A, Surdu AV, Ficai D, Oprea OC, et al. Antibacterial activity of zinc oxide nanoparticles loaded with essential oils. Pharmaceutics. 2023;15(10):2470. doi: 10.3390/pharmaceutics15102470.

17. Barua E, Deoghare AB, Chatterjee S, Sapkal P. Effect of ZnO reinforcement on the compressive properties, *in vitro* bioactivity, biodegradability and cytocompatibility of bone scaffold developed from bovine bone-derived HAp and PMMA. Ceram Int. 2019;45(16):20331–45. doi:10.1016/j.ceramint.2019.07.006.
18. Ahmad N, Ahmad SI, Ahmedi S, Yadav P, Manzoor N, Parwaz M, et al. Structural, optical and antifungal properties of the PMMA-ZnO nanocomposites: potential applications in odontology. Mater Chem Phys. 2023;309:128382. doi:10.1016/j.matchemphys.2023.128382.
19. Ben Aissa C, Barhoumi N, Khlifi K, Bousslama W, Karkouch I, Majid F. Nanocomposite dental restorations resin doped with smart antimicrobial agents: mechanical properties, wear resistance and antimicrobial activities. Mater Today Commun. 2025;48:113489. doi:10.1016/J.MTCOMM.2025.113489.
20. Rehner AMG, Tudorache DI, Bîrcă AC, Nicoară AI, Niculescu AG, Holban AM, et al. Antibacterial properties of PMMA/ZnO(NanoAg) coatings for dental implant abutments. Materials. 2025;18(2):382. doi:10.3390/ma18020382.
21. Ponnamma D, Cabibihan JJ, Rajan M, Pethaiah SS, Deshmukh K, Gogoi JP, et al. Synthesis, optimization and applications of ZnO/polymer nanocomposites. Mater Sci Eng C. 2019;98:1210–40. doi:10.1016/j.msec.2019.01.081.
22. Liu J, Ma J, Bao Y, Wang J, Zhu Z, Tang H, et al. Nanoparticle morphology and film-forming behavior of polyacrylate/ZnO nanocomposite. Compos Sci Technol. 2014;98(4):64–71. doi:10.1016/j.compscitech.2014.02.019.
23. Algamdi B, Alam MM, Tashkandi N, Bahaidarah EA, Alshareef FM, Alzahrani KA, et al. New furan-cross-linked PMMA for efficient removal of cationic dyes and detection of cadmium ions. Polym Adv Technol. 2025;36(2):e70107. doi:10.1002/pat.70107.
24. Hammani S, Barhoum A, Bechelany M. Fabrication of PMMA/ZnO nanocomposite: effect of high nanoparticles loading on the optical and thermal properties. J Mater Sci. 2018;53(3):1911–21. doi:10.1007/s10853-017-1654-9.
25. Permyakova ES, Manakhov AM, Kiryukhantsev-Korneev PV, Leybo DV, Konopatsky AS, Makarets YA, et al. Electrospun polycaprolactone/ZnO nanocomposite membranes with high antipathogen activity. Polymers. 2022;14(24):5364. doi:10.3390/polym14245364.
26. Alamgeer, Tahir M, Sarker MR, Ali S, Ibraheem, Hussian S, et al. Polyaniline/ZnO hybrid nanocomposite: morphology, spectroscopy and optimization of ZnO concentration for photovoltaic applications. Polymers. 2023;15(2):363. doi:10.3390/polym15020363.
27. Zhang Y, Zhuang S, Xu X, Hu J. Transparent and UV-shielding ZnO@PMMA nanocomposite films. Opt Mater. 2013;36(2):169–72. doi:10.1016/j.optmat.2013.08.021.
28. Farha AH, Al Naim AF, Mansour SA. Thermal degradation of polystyrene (PS) nanocomposites loaded with sol gel-synthesized ZnO nanorods. Polymers. 2020;12(9):1935. doi:10.3390/polym12091935.
29. Ng AMC, Chan CMN, Guo MY, Leung YH, Djurišić AB, Hu X, et al. Antibacterial and photocatalytic activity of TiO_2 and ZnO nanomaterials in phosphate buffer and saline solution. Appl Microbiol Biotechnol. 2013;97(12):5565–73. doi:10.1007/s00253-013-4889-7.
30. Rodrigues AS, Batista JGS, Rodrigues MÁV, Thipe VC, Minarini LAR, Lopes PS, et al. Advances in silver nanoparticles: a comprehensive review on their potential as antimicrobial agents and their mechanisms of action elucidated by proteomics. Front Microbiol. 2024;15:1440065. doi:10.3389/fmicb.2024.1440065.
31. Gudkov SV, Burmistrov DE, Fomina PA, Validov SZ, Kozlov VA. Antibacterial properties of copper oxide nanoparticles (review). Int J Mol Sci. 2024;25(21):11563. doi:10.3390/ijms252111563.
32. Abd El-Kader MFH, Elabbasy MT, Adeboye AA, Zeariya MGM, Menazea AA. Morphological, structural and antibacterial behavior of eco-friendly of ZnO/TiO_2 nanocomposite synthesized via *Hibiscus* rosa-sinensis extract. J Mater Res Technol. 2021;15(5):2213–20. doi:10.1016/j.jmrt.2021.09.048.
33. de Lima MS, Schio AL, Aguzzoli C, de Souza WV, Roesch-Ely M, Leidens LM, et al. Visible light-driven photocatalysis and antibacterial performance of a Cu-TiO_2 nanocomposite. ACS Omega. 2024;9(47):47122–34. doi:10.1021/acsomega.4c07515.
34. Govindasamy GA, Mydin RBSMN, Gadaime NKR, Sreekantan S. Phytochemicals, biodegradation, cytocompatibility and wound healing profiles of chitosan film embedded green synthesized antibacterial ZnO/CuO nanocomposite. J Polym Environ. 2023;31(10):4393–409. doi:10.1007/s10924-023-02902-1.

35. Gouyau J, Duval RE, Boudier A, Lamouroux E. Investigation of nanoparticle metallic core antibacterial activity: gold and silver nanoparticles against *Escherichia coli* and *Staphylococcus aureus*. Int J Mol Sci. 2021;22(4):1905. doi:10.3390/ijms22041905.
36. Modi SK, Gaur S, Sengupta M, Singh MS. Mechanistic insights into nanoparticle surface-bacterial membrane interactions in overcoming antibiotic resistance. Front Microbiol. 2023;14:1135579. doi:10.3389/fmicb.2023.1135579.
37. More PR, Pandit S, De Filippis A, Franci G, Mijakovic I, Galdiero M. Silver nanoparticles: bactericidal and mechanistic approach against drug resistant pathogens. Microorganisms. 2023;11(2):369. doi:10.3390/microorganisms11020369.